Plasmon Enhanced Photocurrent in Strong Coupling Ag@Perylene Core-Shell Nanowires

Journal:	*Journal of Materials Chemistry A*
Manuscript ID:	TA-ART-03-2015-001772.R1
Article Type:	Paper
Date Submitted by the Author:	29-Apr-2015
Complete List of Authors:	Lin, Ling; Hefei National Laboratory for Physical Sciences at Microscale, University of Science and Technology of China, Division of Nanomaterials and Chemistry Gao, Guiqi; Anhui University, Modern Experiment Technology Center Zhu, Qing; Hefei National Laboratory for Physical Sciences at Microscale, University of Science and Technology of China, Division of Nanomaterials and Chemistry Xu, An-Wu; Hefei National Laboratory for Physical Sciences at Microscale, University of Science and Technology of China, Division of Nanomaterials and Chemistry

SCHOLARONE™
Manuscripts

Paper

Plasmon Enhanced Photocurrent in Strong Coupling Ag@Perylene Core-Shell Nanowires

Ling Lin[a], Gui-Qi Gao[a, b], Qing Zhu[a] and An-Wu Xu*[a]

5

Plasmon hot electron injection enhanced photocurrent has
10 potential applications in light harvesting in photovoltaic devices.
We demonstrate a cathodic photocurrent enhancement system
utilizing strongly coupled Ag@Perylene (Ag@Pe) core-shell
nanowires, and the perylene shell thickness can be readily
controlled. The strong coupling between plasmonic resonance
15 and molecular exciton resonance is evidenced by the substantial
plasmon damping of Ag NWs and the enhancement of
fluorescence of perylene with a red shift in Ag@Pe samples. The
photocurrent of Ag@Pe sample with the shell thickness of 5.8 nm
(Ag@Pe-5.8 nm) shows a 16-fold enhancement compared to that
20 of perylene. While, simply-mixed Ag-perylene sample displays
only a 6-fold enhancement in photocurrent, indicating that the
strong coupling in Ag@Pe system plays a major role in the
enhancement of photocurrent through hot electron transfer from
the silver nanowires to perylene molecules. This strongly coupled
25 Ag@Pe hetero-nanostructure could find potentials in surface
plasmon-driven, hot-electron solar cells and surface catalytic
reactions.

Introduction

30

Noble metal nanocrytals have been well-investigated for their
localized surface plasmon resonances (LSPRs), which will
largely enhance the electromagnetic field near the nanocrytals
based on resonant excitation. In terms of the prospect that LSPRs
35 will afford significant applications in photonic devices,[1]
biological imaging and sensing,[2,3] and photoelectric conversion
devices,[4,5] numerous studies focused on the interaction between
plasmonic metal nanocrystals and organic molecules have been
carried out.[6–9] Noble metal nanocrystals can electromagnetically
40 interact with the adsorbed organic molecules, which are verified
from the plasmon-enhanced absorption and emission,[10,11]
fluorescence quenching,[12] plasmon-enhanced nonlinear optical
processes[13] and surface enhanced Raman scattering (SERS)[14,15].
Strong coupling between plasmon and molecular resonance of
45 absorbed organic molecules occurs when there exists a large
spectral overlap between plasmonic resonance and molecular
resonance. Under such a strong coupling condition, the electronic

excitation of surface-adsorbed molecules was substantially
enhanced, and the enhanced excitation can in turn influence the
50 plasmon resonance of metal nanocrystals.[9,16]

Once a plasmonic mode has been excited, plasmons can
decay nonradiatively by transferring the accumulated energy to
electrons in the conduction band of the nanocrystals and produce
hot electrons.[17–20] Recent researches have demonstrated that hot
55 electrons can be collected by a metal–semiconductor Schottky
junction, which provide a way to investigate hot-electron solar
cells.[20–22] Besides, when a molecule is strong coupled with
plamon, hot-electron transfer from a metal to an unoccupied
molecular orbital at the surface could also occur.[23,24] Recently,
60 the plasmon-molecule coupling has been applied to enhance
photocurrent responses in optoelectronic devices and
nanostructures.[25–28] Plasmonic enhancement of photocurrents can
be induced via direct electron transfer from a metal or indirectly
via a local amplification of electromagnetic field. Improvement
65 of the optoelectronic conversion efficiency is very important to
the performance of organic photovoltaics (OPVs), in which
organic dyes or polymers are utilized as light absorption
materials.[29,30] Therefore, studies on the enhanced optoelectronic
responses of organic dyes caused by LSPRs of noble metal
70 nanocrystals are of great significance for designing more efficient
photoelectric conversion devices.

In this work, we describe the construction of an efficient
optoelectronic conversion and photocurrent enhancement system
which can effectively use the plasmon hot electrons. Perylene is
75 chosen as the photo-response molecules, because perylene
derivatives (perylene imides and perylene anhydrides) are widely
used in OPVs due to their high fluorescence quantum yield,
molar absorption constant and chemical stability,[31–33] and
researches on the optoelectronic response of perylene core
80 provide us better understanding and design of perylene
derivatives based OPVs. To design effective plasmon based
molecular optoelectronic conversion systems, the first step is to
fabricate an electrode with a molecularly organized layers on
metal nanoparticle surface. Self-assembled monolayers (SAMs)
85 method is the most invstigated approach to fabricate well-defined
monolayer with self-organization property on noble metal
nanoparticles to date.[26,34] However, SAMs method also suffers
from a lack of control over the thickness of organic dyes
adsorbed on metal nanoparticles. In addition, metal nanocrystals
90 employed in SAMs method are attached on substrates, which
makes it difficult to uniformly cover around each metal
nanoparticle with organic molecules. As an alternative approach,
we develop a photocurrent enhancement system based on
Ag@perylene core–shell nanowires (Ag@Pe NWs) prepared by
95 an *in-situ* reaction between Ag nanowires (Ag NWs) and
perylene cation radicals (Pe$^+$). The perylene shell thickness can

[a]Division of Nanomaterials and Chemistry, Hefei National Laboratory for
Physical Sciences at Microscale, Department of Chemistry, University of
Science and Technology of China, Hefei 230026, P. R China.
Fax: (+86) 551-6360 2346; E-mail: anwuxu@ustc.edu.cn.
[b]Modern Experiment Technology Center, Anhui University, Hefei, Anhui
230601, P. R China.
† Electronic Supplementary Information (ESI) available: [details of any
supplementary information available should be included here]. See
http://dx.doi.org/10.1039/b000000x/

be controlled by varying the amount of initial perylene cation radicals. The enhanced electric field resulting from LSPRs of Ag NWs can have an effect on the photocurrent of perylene. What's more, the molecular resonance of perylene is degenerate with the plasmonic resonance of Ag NWs, leading to a strong coupling between Ag NWs and perylene molecules, and hot-electron transfer from Ag NWs to lowest unoccupied molecular orbital (LUMO) energy level[35] of perylene. In the present work, we examined the effect of plasmonic hot electrons on the photocurrents of the Ag@Pe NWs films and relationship between perylene shell thickness and the enhancement of photocurrents.

Experimental Section

Materials

Perylene (Pe) was purchased from Aladdin Reagents Co., Ltd. and silver perchlorate was purchased from Alfa Aesa. Silver nitrate, poly (vinyl pyrrolidone) (PVP, K-30), ethylene glycol (EG), sodium chloride, anhydrous acetonitrile, dichloromethane and anhydrous sodium sulfate were purchased from Sinopharm Chemical Reagent Co., Ltd. All reagents were used as received without further purification.

Characterizations

The scanning electron microscope (SEM) images and transmission electron microscope (TEM) images were taken using a field-emission scanning electron microscope (JSM-6701F, JEOL) operated at an accelerating voltage of 5 kV and a JEOL-2010 transmission electron microscope at an operation voltage of 100 kV, respectively. The UV−visible spectra were recorded on a HITACHI U-3900 double-beam recording spectrophotometer (0.5 nm resolution). Electrochemical measurements were carried out on a CHI660D potentiostat (Shanghai Chen Hua Instrument Co., Ltd).

Synthesis of Ag NWs and Pe$^{\bullet+}$

The silver nanowires were prepared by a modified polyol process.[36] In a typical synthesis, 1, 2-Propylene glycol (1, 2-PG, 10mL) that contained poly (vinyl pyrrolidone) (PVP, 150 mM) was placed in a 25-mL vial, capped, and heated with stirring in an oil bath at 160 ºC for 1 h. 1 mL NaCl solution (1 mM in 1, 2-PG) was then quickly added. After 5 min, AgNO$_3$ (0.15 M solution in 1, 2-PG, 4 mL) were added to the stirring solution dropwise. The vial was then capped and heated at 160 ºC for 40 min. After injection of the AgNO$_3$ solution, the color of reaction mixture changed from milkiness to light yellow, and silvery white. After cooling to room temperature, the products were all purified by centrifugation to remove PVP with ethanol for several times. The products were dried in vacuum at 70 ºC overnight and then dispersed in anhydrous acetonitrile (5 mM) for further experiments.

To a 10 mL methylene chloride solution of 0.14 M perylene was added a solution of 290 mg of dry silver perchlorate in a minimum of acetonitrile under nitrogen. After stirring for 5 min, a solution of 177 mg of iodine in a minimum of methylene chloride was added to the mixture. A dark precipitate formed immediately. The precipitate was filtered, washed with methylene chloride and dried under vacuum, giving a solid of PeClO$_4$/AgI. 0.587 mg of PeClO$_4$/AgI was put in a test tube with tinfoil to keep out of the light, then 10 mL of acetonitrile was added dropwise to obtain a 0.1 mM solution of PeClO$_4$.

Preparation of Ag@Pe NWs

A series of different volumes (0.025−0.20 mL) of 0.1 mM Pe$^{\bullet+}$ClO4$^-$ solution in anhydrous acetonitrile were added to 1 mL of a 5 mM Ag NWs suspension in anhydrous acetonitrile under vigorous stirring. After synthesis, the suspension was centrifugated, washed with acetonitrile and redispersed in 1 mL acetonitrile for further use.

Fabrication of Ag@Pe NWs films

The indium-tin oxide (ITO) substrates (surface resistivity: 10 Ω/sq, 15×20 mm) were cleaned with acetone and ethanol and then drying with the nitrogen gas before use. Ag@Pe NWs films were fabricated by a drop-casting method. A 100 μL suspension of Ag@Pe in acetonitrile was drop casted onto the ITO substrate and dried in a 60ºC oven. After repeating the drop-casting process for another two times, the films were left in a 60ºC oven over night. The control sample of simply mixing of Ag NWs and perylene was prepared by drop-casting 100 μL of perylene solution after a layer of 100 μL Ag NWs, the process was repeated another two times. Pure perylene films (Pe films) were prepared by the same drop-casting method for three times using perylene acetonitrile solutions with different concentrations (0.0025 mM−0.02 mM).

Photocurrent measurement

Photocurrent measurements were carried out in an aqueous solution containing 0.1 M Na$_2$SO$_4$ using Ag/AgCl (sat. KCl) and platinum as reference and counter electrode, respectively. The visible light (> 400 nm) from a Xe lamp with a light filter irradiated the working electrode, and the resultant photocurrents were measured with a CHI660D electrochemical workstation. All photocurrents were measured at E = −0.2 V versus Ag/AgCl.

Results and discussion
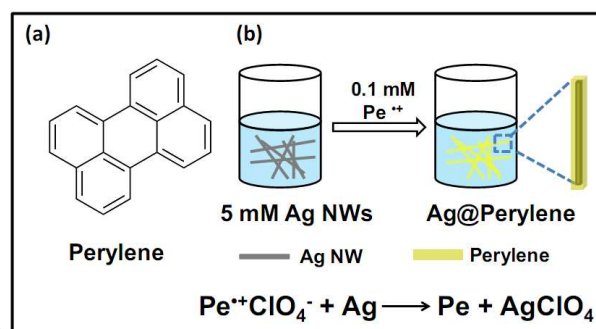
Scheme 1. (a) Chemical structure of perylene. (b) Schematic illustration of the in situ growth of perylene on the Ag NWs.
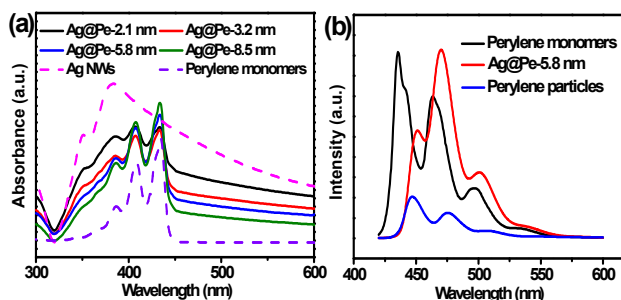
The first redox potential of perylene in acetonitrile is 1.01 V,[37] which is higher than that of Ag (0.79 V), hence, perylene cation radical (Pe$^{\bullet+}$) can be easily reduced to neutral perylene by Ag when Pe$^{\bullet+}$ is added to the dispersion of Ag NWs. On the basis of this redox reaction, Ag@Pe NWs are fabricated by an in situ growth route (Scheme 1).[38] Perylene cation radical was prepared by oxidation of perylene in dichloromethane in the presence of silver perchlorate (AgClO$_4$) using iodine as the oxidant.[39] Pe$^{\bullet+}$ClO$_4$$^-$ acetonitrile solution (0.1 mM) with various amounts (0.025−0.20 mL) were added to Ag NWs dispersion with different concentration and volume to make sure the concentration of

Journal of Materials Chemistry A

perylene in the mixture varied from 0.0025 mM to 0.020 mM, and the concentration of Ag NWs suspension was kept constant at 5 mM. The purple color of the $Pe^{•+}ClO_4^-$ vanished immediately and the color of the Ag NWs suspension turned grayish yellow, indicating the reduction of $Pe^{•+}$ to perylene. The resulting perylene grew on the Ag NW surface to form a shell due to the solubility in acetonitrile of neutral perylene is lower than that of $Pe^{•+}$. The scanning electron microscopy (SEM) image of Ag@Pe (Fig. 1b) shows that the morphology of the Ag NWs encapsulated by perylene is almost the same as bare Ag NWs (Fig. 1a), indicating that perylene forms thin shells around Ag NWs. Meanwhile, a clear shell of perylene can be found in the transmission electron microscopy (TEM) image of an individual Ag@Pe NWs (Fig. 1c), signifying the formation of Ag@Pe core-shell nanowires. Energy-dispersive X-ray spectroscopy (EDS) analysis verifies that the Ag@Pe sample contains the elements of Ag and C (Fig. S1). Elemental mapping images of the same nanowire region (Fig. 1d) further confirm the perylene shell formed on each Ag NW, and the uniform distribution of C element suggests that the perylene molecules uniformly coat on the Ag NWs. The perylene shell thickness can be easily tuned by varying the amount of $Pe^{•+}$ added to the Ag NWs dispersion. According to the TEM results (Fig. S2), it can be seen that the perylene shell thickness increases with the increasing amount of $Pe^{•+}$. At low concentration of $Pe^{•+}$ (< 0.005 mM), the perylene shell thickness does not show an obvious increase, because the small amount of generated perylene dissolves in acetonitrile due to the critical value of solubility of perylene. As the $Pe^{•+}$ concentration increased from 0.005 to 0.020 mM, a distinct increase in shell thickness from 2.1 to 8.5 nm is clearly observed (Fig. S2a−d). The adjustable perylene shell thickness facilitates us to investigate the optoelectronic response of perylene coating on plasmonic Ag NWs. Ag 3d XPS and Ag MNN Auger spectra of Ag@Pe-5.8 nm are shown in Fig. S3. The XPS spectra of Ag 3d can be further divided into four peaks (373.9, 373.5 eV, and 367.9, 367.5 eV), peaks at 367.9 and 373.9 eV can be attributed to Ag(0), whereas peaks at 367.5 and 373.5 eV can be attributed to Ag(I). Ag MNN spectrum shows three peaks at 358.6, 352.6 eV and a shoulder peak at 353.7. Among them, the shoulder peak at 353.7 eV is ascribed to the reported Ag(I) species,[40] suggesting the presence of Ag(I) on the surface of Ag. In addition, when NaCl solution was added to the supernatant of Ag@Pe-5.8 nm after centrifugation, white precipitates were observed, indicating most of the Ag(I) cations enter into the solution.
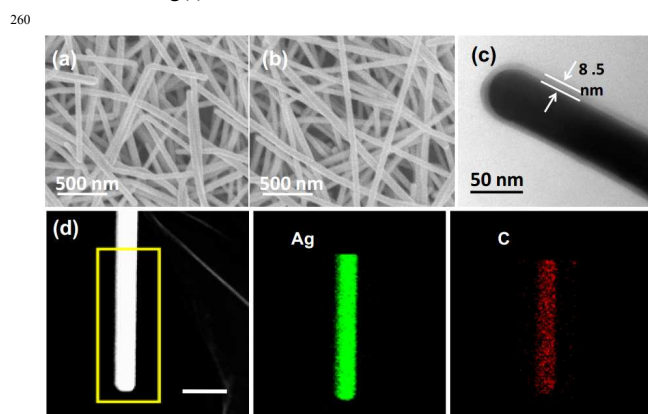
Fig. 2a shows the UV-visible absorption spectra of Ag NW dispersion, perylene monomers in acetonitrile and Ag@Pe samples with different perylene shell thickness. The absorption spectrum of Ag NWs solution (the dashed magenta line) displays a broad band from 320 nm extending to the visible light region with the appearing of two distinct characteristic peaks at 350 and 382 nm, which are ascribed to the bulk surface plasmon resonance of Ag NWs and the transverse plasmon mode, respectively.[41] The absorption spectrum of perylene monomers in acetonitrile shows three typical peaks at 386, 406 and 433 nm (the dashed violet line). It can be observed that there exists a large overlap between plasmonic resonance of Ag NWs and molecular resonance of perylene. The UV-visible absorption spectra of Ag@Pe samples show no obvious shift of the absorption peaks of perylene, however, the LSPRs of Ag NWs exhibits obvious damping, confirming the coupling between Ag NWs and perylene molecules. Also, the fluorescence spectra of perylene monomers and Ag@Pe samples were measured (Fig. 2b). The fluorescence of Ag@Pe-5.8 nm (the shell thickness is 5.8 nm) is red-shifted with respect to perylene monomers, which can be attributed to the formation of excimers in the aggregated state. When a monomer molecule is electronically excited, it would couple with the neighbor unexcited fluorophore; leading to the formation of excimers. Excimers could cause the energy level increase of the ground state and the energy level decrease of the excited state compared to the monomer species, thus, inducing a red shift of the aggregate fluorescence.[42,43] The intensities of the fluorescence of Ag@Pe samples increase with the shell thickness increasing (Fig. S4). More importantly, the fluorescent intensity of Ag@Pe-5.8 nm is higher than that of pure perylene aggregate particles formed by adding 0.15 mL 0.1 mM perylene to 0.5 M cetyltrimethylammonium bromide (CTAB) aqueous solution. The fluorescence enhancement can be mainly attributed to near-field enhancement and the energy transfer from Ag NWs to perylene shells.[44,45] The substantial plasmon damping of Ag NWs and enhancement of fluorescence of perylene in Ag@Pe samples with a red shift provide a clear evidence for the strong coupling in Ag@Pe core-shell nanostructures.

Figure 1. SEM image of (a) Ag NWs, (b) Ag@Pe NWs formed by injection of 0.2 mL $Pe^{•+}$ (the concentration of $Pe^{•+}$ is 0.02 mM). (c) TEM image of the end of an individual Ag@Pe NW with 0.2 mL $Pe^{•+}$. (d) Dark-field TEM image of the end of an individual Ag@Pe NW with 0.2 mL $Pe^{•+}$ and the elemental mapping of the same region. The scale bar is 100 nm.

Figure 2. (a) UV-visible absorption spectra of Ag NW dispersion, perylene monomers in acetonitrile and Ag@Pe samples with different perylene shell thickness. (b) Fluorescence spectra of perylene monomers, Ag@Pe-5.8 nm sample and pure perylene aggregate particle dispersion.

To investigate the optoelectronic response of Ag@Pe NWs, we fabricated the work electrodes by drop-casting Ag@Pe NW dispersions onto ITO substrates. Fig. S5b shows the low magnification SEM image of Ag@Pe NWs film drop-casted on ITO substrate. It is clear that drop-casting can form relatively uniform Ag@Pe NWs film. The inset pictures of ITO substrates before (left) and after (right) drop-casting of Ag@Pe also confirm the formation of uniform transparent films. For control experiments, pure Ag NWs and perylene work electrodes were

also fabricated by the same drop-casting method. The SEM image of Pe film prepared by drop-casting of 0.02 mM Pe solution is shown in Fig. 5Sa, indication that perylene molecules form a continuous and uniform film. The photocurrent–voltage behavior of perylene and Ag@Pe-5.8 nm samples observed under visible light (> 400 nm) illumination is shown in Fig. 3a. As shown in the inset of Fig. 3a, a magnification of the voltage range between −0.35 to 0.15 V, both perylene and Ag@Pe-5.8 nm samples show a cathodic photocurrent at applied zero bias voltage *vs* Ag/AgCl reference electrode, indicating that electrons transfer from the film to the electrolyte during light irradiation; and the short-circuit photocurrent density for Ag@Pe-5.8 nm sample is much larger than the pure perylene sample. An obvious increase in the cathodic photocurrent beginning at a bias voltage of −0.2 V can be observed for Ag@Pe-5.8 nm sample, while the sharp increase of photocurrent occurs at a bias voltage of −0.58 V for perylene-only film. Thus, the presence of Ag NWs plasmonic significantly enhances the optoelectronic performance of our Ag@Pe photocathode. Fig. 3b shows the time-dependent photocurrent of perylene and Ag@Pe-5.8 nm samples at a bias voltage of −0.2 V. For perylene film without Ag NWs, a small cathodic photocurrent density of 0.04 μA cm^{-2} is obtained. However, a 16-fold enhancement in the photocurrent is evident for the Ag@Pe-5.8 nm sample, namely, 0.8 μA cm^{-2} by subtracting the photocurrent of pure Ag NWs (Fig. S6).
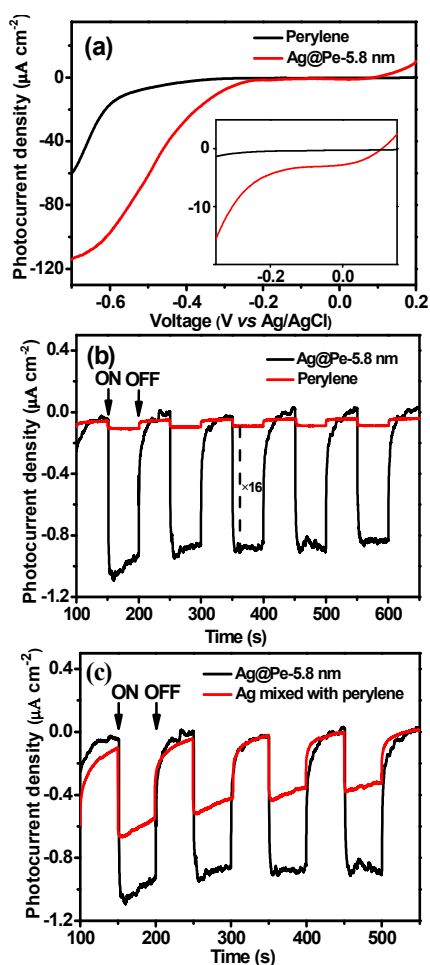
Figure 3. (a) Photocurrent–voltage behavior of perylene and Ag@Pe-5.8 nm sample measured under visible light (> 400 nm) illumination. (b) Time-dependent photocurrent of perylene and Ag@Pe-5.8 nm samples at

a bias voltage of −0.2 V. (c) Time-dependent photocurrent of Ag@Pe-5.8 nm and Ag NWs simply mixed with perylene samples.

The significantly enhanced photocurrent observed from our Ag@Pe core-shell nanostructures could be due to the electric field enhancement caused by plasmonic effects, higher surface area of Ag@Pe film as compared to Pe film and hot electron contribution of Ag NWs because of the strong coupling between Ag NWs and perylene molecules. To investigate the influence of different factors on the photocurrent enhancement, photocurrent of the control sample of Ag NWs simply mixed with perylene was also measured. We observed a photocurrent density of ~0.3 μA cm^{-2} of the simply-mixed Ag-perylene sample (Fig. 3c), which shows a 6-fold enhancement in photocurrent as compared to pure perylene. This result suggests that the enhanced electric fields resulting from LSPRs and have an influence on the enhancement of photocurrent signals, as observed by previous works.[46,47] Besides, the influence of higher surface area of Ag@Pe film compared to Pe film is also an important aspect that can not be neglected, because high surface area could lead to a high contact area between electrode and electrolyte, thus facilitates the transfer of electrons.[48,49] More importantly, our Ag@Pe 5.8 nm sample has a 16-fold enhancement, quite higher than simply mixed sample, which has electric field enhancement and high surface area, indicating that the strong coupling between Ag NWs and perylene molecules plays a major role in the higher enhancement of photocurrent in Ag@Pe-5.8 nm sample. In our strong coupled Ag@Pe system, the hot electrons generated by Ag NWs under light irradiation can transfer to the LUMO energy level of perylene molecules and then contribute to the photocurrent of Ag@Pe,[23] which is in accordance with the enhancement of fluorescence.
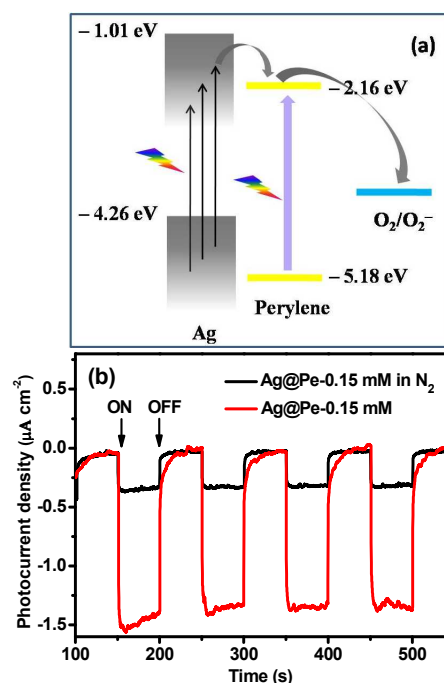
Figure 4. (a) Schematic diagram of the electron transfer procedure in the system of Ag@Pe core-shell nanowires. (b) Photocurrent of Ag@Pe-5.8 nm sample with and without bubbling of nitrogen.

From the above, we propose a reasonable mechanism for this photoelectrochemical process (Fig. 4a). Electron-transfer started from the photo-excitation of perylene molecules, and then

electrons transfer from the photoexcited perylene to oxygen molecules dissolved in the aqueous solution. At the same time, hot electrons of the excited Ag NWs transfer across metal-organic interfaces to the LUMO energy level of perylene molecules. As a result, a cathodic photocurrent is observed. This oxygen-assisted reaction has been well documented in the cases of Ag and Au nanoparticles enhanced photocurrents of porphrins on electrodes.[34] To prove that oxygen participated in the photochemical reactions, the control experiment by bubbling the electrolyte solution with nitrogen for 10 minutes was carried out. Fig. 4b shows that deoxygenization by nitrogen leads to a decrease of the photocurrent density by 75%, thus confirming oxygen-mediated photochemical process.
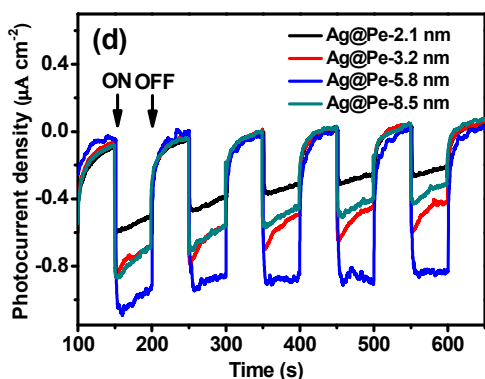
Figure 5. Time-dependent photocurrent of Ag@Pe samples with different shell thickness.

Effects of perylene shell thickness on photocurrents also demonstrate the hot electrons generated from Ag NWs make much contribution to photocurrent enhancement (Fig. 5). When the shell thickness reaches 5.8 nm, the extraction of plasmon hot electrons by perylene is so sufficient that the photocurrent is already maximized at this shell thickness. With the shell thickness decreasing, the extraction of plasmon hot electrons by perylene is not so much sufficient, and the contribution of perylene itself is also small, therefore, the photocurrent decreases. When the shell thickness is over 5.8 nm, the photocurrent decreases, which is likely due to the more absorption of light and light shielding effect by thicker perylene that decreases the light irradiation on Ag NWs; consequently, the number of hot electrons transferring from excited Ag NWs to perylene molecules decrease. As a control experiment, pure perylene films with different amount were fabricated, and their photocurrents were measured. Fig. S7 shows that the photocurrents increase with an increase of the amount of perylene. The different photocurrent behavior of Ag@Pe samples and pure perylene samples manifests that Ag NWs plays a major role in the photocurrent enhancement of perylene, and that the optimum perylene shell thickness is 5.8 nm, with a photocurrent enhancement factor of 16 for Ag@Pe-5.8 nm core-shell nanowires.

Conclusions

We have developed a photocurrent generation system of Ag@Pe nanowires formed by an *in-situ* reaction between Ag NWs and perylene radical cations. Highly enhanced photocurrent is observed, which is maily contributed by plasmonic hot electron transfer from Ag NWs to perylene. The perylene shell thickness of Ag@Pe NWs can be controlled by varying the amount of initiating perylene cation radicals. Strong plasmon-molecule coupling occurs in Ag@Pe core-shell nanostructure, resulting in plasmon damping of Ag NWs and the enhancement of fluorescence of perylene in Ag@Pe samples with a red shift. The coupling effect induces a great photocurrent enhancement of Ag@Pe samples due to the contribution of hot electrons of excited Ag NWs transferring to perylene molecules. Photocurrent measurements also show that the shell thickness has a great effect on the photocurrents of Ag@Pe samples, and the optimum thickness is 5.8 nm, yielding a 16-fold in the photocurrent. Our results could be extended for designing more efficient systems with plasmonic enhancement for optoelectronic conversion devices, such as plasmonic solar cells.

Notes and references

‡ Additional fig.s are given in supporting information.

1 E. Ozbay, *Science* 2006, **311**, 189−193.

2 K. M. Mayer and J. H. Hafner, *Chem. Rev.* 2011, **111**, 3828–3857.

3 W.-G. Qu, S.-M. Wang, Z.-J. Hu, T.-Y. Cheang, Z.-H. Xing, X.-J. Zhang and A.-W. Xu, *J. Phys. Chem. C* 2010, **114**, 13010–13016.

4 H. A. Atwater and A. Polman, *Nat. Mater.* 2010, **9**, 205−213.

5 P. Du, P. Jing, D. Li, Y. Cao, Z. Liu andZ. Sun, *Small* 2015, DOI: 10.1002/smll.201402757.

6 N. Passarelli, L. A. Pérez, and E. A. Coronado, *ACS Nano* 2014, **8**, 9723−9728.

7 G. P. Wiederrecht, G. A. Wurtz and J. Hranisavljevic, *Nano Lett.* 2004, **4**, 2121−2125.

8 B. K. Juluri, M. Lu, Y. B. Zheng, T. J. Huang and L. Jensen, *J. Phys. Chem. C* 2009, **113**, 18499–18503.

9 W. Ni, T. Ambjörnsson, S. P. Apell, H. Chen and J. Wang, *Nano Lett.* 2010, **10**, 77–84.

10 V. Giannini, A. I. Fernández-Domínguez, S. C. Heck and S. A. Maier, *Chem. Rev.* 2011, **111**, 3888−3912.

11 Y. Fu, J. Zhang and J. R. Lakowicz, *J. Am. Chem. Soc.* 2010, **132**, 5540–5541.

12 G. Schneider, G. Decher, N. Nerambourg, R. Praho, M. H. V. Werts and M. Blanchard-Desce, *Nano Lett.* 2006, **6**, 530–536.

13 K. Ueno, S. Juodkazis, T. Shibuya, Y. Yokota, V. Mizeikis, K. Sasaki and H. Misawa, *J. Am. Chem. Soc.* 2008, **130**, 6928−6929.

14 A. Campion and P. Kambhampati, *Chem. Soc. Rev.* 1998, **27**, 241–250.

15 L. Q. Lu, Y. Zheng, W. G. Qu, H. Q. Yu and A. W. Xu, *J. Mater. Chem.* 2012, **22**, 20986−20990.

16 G. Wurtz, P. Evans, W. Hendren, R. Atkinson, W. Dickson, R. Pollard, W. Harrison, C. Bower and A. Zayats, *Nano Lett.* 2007, **7**, 1297−1303.

17 A. Furube, L. Du, K. Hara, R. Katoh and M. Tachiya, *J. Am. Chem. Soc.* 2007, **129**, 14852–14853.

18 C. Sönnichsen, T. Franzl, T. Wilk, G. von Plessen and J. Feldmann, *Phys. Rev. Lett.* 2002, **88**, 077402.

19 M. W. Knight, H. Sobhani, P. Nordlander and N. J. Halas, *Science*, 2011, **332**, 702−704.

20 Y. Nishijima, K. Ueno, Y. Yokota, K. Murakoshi and H. Misawa, *J. Phys. Chem. Lett.* 2010, **1**, 2031–2036.

21 F. P. G. Arquer, A. Mihi, D. Kufer and G. Konstantatos, *ACS Nano* 2013, **7**, 3581–3588.

22 C. Clavero *Nat. Photon.* 2014, **8**, 95–103.

23 M. L. Brongersma, N. J. Halas and P. Nordlander, *Nat. Nanotech.* 2015, **10**, 25–34.

515 24 A. O. Govorov, H. Zhang, H. V. Demir and Y. K. Gun'Ko, *Nanotoday*, 2014, **9**, 85–101.

25 T. Akiyama, M. Nakada, N. Terasakiand and S. Yamada, *Chem. Commun.* 2006, **42**, 395–397.

26 R. Matsumoto, H. Yonemura and S. Yamada, *J. Phys. Chem. C* 2013, 520 **117**, 2486−2493.

27 M. A. Mangold, C. Weiss, M. Calame and A. W. Holleitner, *Appl. Phys. Lett.* 2009, **94**, 161104.

28 K. Leonard, J. You, Y. Takahashi, H. Yonemura, J. Kurawaki and S. Yamada, *J. Phys. Chem. C*, 2015, **119**, 8829–8837.

525 29 S.-W. Baek, J. Noh, C.-H. Lee, B. Kim, M.-K. Seo and J.-Y. Lee, *Sci. Rep.* 2013, **3**, 1726.

30 J.-L. Wu, F.-C. Chen, Y.-S. Hsiao, F.-C. Chien, P. Chen, C.-H. Kuo, M. H. Huang and C.-S. Hsu, *ACS Nano* 2011, 5, 959−967.

31 C. Li, M. Y. Liu, N. G. Pschirer, M. Baumgarten and K. Müllen, 530 *Chem. Rev.* 2010, **110**, 6817–6855.

32 X. Zhang, Z. H. Lu, L. Ye, C. L. Zhan, J. H. Hou, S. Q. Zhang, B. Jiang, Y. Zhao, J. H. Huang, S. L. Zhang, Y. Liu, Q. Shi, Y. Q. Liu and J. N. Y ao, *Adv. Mater.* 2013, **25**, 5791–5797.

33 G. D. Sharma,; P. Suresh, J. A. Mikroyannidis and M. M. Stylianakis, 535 *J. Mater. Chem.* 2010, **20**, 561–567.

34 K. Kanaizuka, S. Yagyu, M. Ishizaki, H. Kon, T. Togashi, M. Sakamoto and M. Kurihara, *Appl. Phys. Lett.* 2012, **101**, 063103.

35 G. J. Zhao and K. L. Han, *J. Phys. Chem. A*, 2009, **113**, 4788–4794.

36 Y. Bi, H. Hu and G. Lu, *Chem. Commun.*, 2010, **46**, 598–600.

540 37 R. M. Young, S. M. Dyar, J. C. Barnes, M. Juríček, J. F. Stoddart, D. T. Co and M. R. Wasielewski, *J. Phys. Chem. A*, 2013, **117**, 12438−12448.

38 X. K. Zhang, L. M. Fu, J. F. Liu, Y. Kuang, L. Luo, D. G. Evans and X. M. Sun, *Chem. Commun.*, 2013, **49**, 3513–3515.

545 39 L. Kang, Z. Wang, Z. Cao, Y. Ma, Fu, H. and J. Yao, *J. Am. Chem. Soc.*, 2007, **129**, 7305−7312.

40 G. Zhu, C. Bao,Y. Liu, X. Shen, C. Xi, Z. Xu and Z. Ji, *Nanoscale* 2014, **6**, 11147–11156.

41 Y. Sun, B. Gates, B. Mayers and Y. Xia, *Nano Lett.*, **2002**, **2**, 550 165−168.

42 L. Zhao, W. Yang, Y. Ma, J. Yao, Y. Li and H. Liu, *Chem. Commun.*, 2003, **39**, 2442–2443.

43 X. Zhang, X. Zhang, W. Shi, X. Meng, C. Lee and S. Lee, *J. Phys. Chem. B*, 2005, **109**, 18777–18780.

555 44 C. Wang, Y. Kuang, L. Luo and X. M. Sun, *J. Mater. Chem. C*, 2013, **1**, 4146−4152.

45 Z. C. Dong, X. L. Zhang, H. Y. Gao, Y. Luo, C. Zhang, L. G. Chen, R. Zhang, X. Tao, Y. Zhang, J. L. Yang and J. G. Hou, *Nat. Photon.*, 2010, **4**, 50−54.

560 46 R. Chakraborty, F. Greullet, C George, D. Baranov, E. D.Fabrizio and R. Krahne, *Nanoscale*, 2013, **5**, 5334–5340.

47 N. Sakai, Y. Fujiwara, Y. Takahashi and T. Tatsuma, *ChemPhysChem*, 2009, **10**, 766–769.

48 P. Staiti, M. Minutoli, F. Lufrano, *Electrochim. Acta* 2002, **47**, 2795– 565 2800.

49 S. P. Jiang, J. G. Love, L. Apateanu, *Solid State Ionics* 2003, **160**, 15– 26.

570 **Graphic Abstract:**
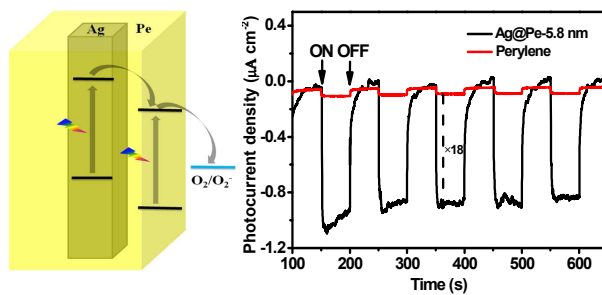
We have developed a hot electron induced photocurrent enhancement system of strong coupling Ag@Perylene core-shell nanowires.